

Rational questing for potential novel inhibitors of FabK from *Streptococcus pneumoniae* by combining FMO calculation, CoMFA 3D-QSAR modeling and virtual screening

Qingye Zhang · Chan Yu · Jun Min · Yan Wang ·
Jin He · Ziniu Yu

Received: 26 April 2010 / Accepted: 2 September 2010 / Published online: 23 September 2010
© Springer-Verlag 2010

Abstract Enoyl-acyl carrier protein (ACP) reductase (ENR) is an attractive and potential target for developing selective antibacterial agents. Recent studies showed that FabK is the sole isoform of ENR in *Streptococcus pneumoniae*, and at the same time an X-ray crystallographic study of FabK from *S. pneumoniae* (SpFabK) was reported for the first time. Based on above information, the interaction mechanism and pair interaction energies between ligand and the active site of SpFabK were analyzed with the *ab initio* fragment molecular orbital (FMO) calculation based on the FlexX docking model at the FMO-RHF/6-31G* level. Subsequently, the first molecular docking-based 3D-QSAR model with comparative molecular field analysis (CoMFA) was established with cross-validated coefficients (q^2) up to 0.511 and regression coefficients (r^2) up to 0.986. Then integrating the 3D-QSAR CoMFA predicted model, molecular docking, and FMO pair interaction analysis structure-based virtual screening was performed, six novel and potential lead compounds were sorted out for further study.

Keywords Enoyl-acyl carrier protein reductase · FabK · Fatty acid biosynthesis · QSAR · Virtual screening

Introduction

Streptococcus pneumoniae is a leading cause of disease and healthcare expenditure worldwide, and it is still a common pathogen of community acquired pneumonia, bacteremia, otitis media and meningitis. The organism claimed the lives of about 3700 people daily, the majority of whom were children below the age of five [1]. With the increasing incidence of penicillin-resistant and macrolide-resistant *S. pneumoniae* strains, deaths increased due to the antibiotics abuse in hospitals [2–4]. Therefore, now it is very urgent to develop new types of antibiotics to overcome this difficult problem, and the effective strategies are to discover new targets or antibacterial agents with novel mechanisms [5].

Fatty acid biosynthesis (FAS) is essential for survival in mammals, plants, fungi and bacteria. Organisms make fatty acids in the assembly of important cellular components including phospholipids, lipoproteins, lipopolysaccharides, mycolic acid, and cell envelope. The FAS of bacteria is catalyzed by a set of distinct, monofunctional enzymes collectively known as the type II FAS (FAS-II). These enzymes differ significantly from the type I FAS (FAS-I) in mammals, in which all of the enzymatic activities are encoded by one or two multifunctional polypeptides. The differences between prokaryote and eukaryote in FAS make this pathway an attractive target for developing selective FAS-II antibacterial agents [6–8]. Enoyl-acyl carrier protein (ACP) reductase (ENR) catalyses the last and rate-limiting step in each round of chain elongation process of FAS-II, and plays a key role in regulation of the pathway [9, 10]. In addition, it shows obvious differences in the overall architecture and low sequence homology with mammalian enzymes [11]. So ENR is a good potential target for selective antibiotics. There are four isoforms, FabI, FabK,

Electronic supplementary material The online version of this article (doi:10.1007/s00894-010-0847-9) contains supplementary material, which is available to authorized users.

Q. Zhang · C. Yu · J. Min · Y. Wang · J. He · Z. Yu (✉)
State Key Laboratory for Agricultural Microbiology and National
Engineering Research Centre of Microbial Pesticides,
Huazhong Agricultural University,
Wuhan 430070, People's Republic of China
e-mail: yzn41@yahoo.cn

FabL and FabV, of ENR [8], and several clinical pathogens contain more than one isoform of ENR, such as *Enterococcus faecalis* and *Pseudomonas aeruginosa* [12]. In such case, inhibitors that target only one isoform of ENR would not be able to inhibit the growth of pathogens. Fortunately, recent genomic studies have shown that FabK is the sole isoform of ENR in *S. pneumoniae*. So FabK will be an excellent target for developing antibacterial agents against *S. pneumoniae*.

The development of novel FabI inhibitors has been reported by several groups [13–20]. The antibacterial agents isoniazid [21], diazaboranes [22, 23], and triclosan [24–28] have been reported as inhibitors of FabI, but many studies validated that these agents showed little inhibitory activity to the FabK target. Furthermore, only a few inhibitors of the FabK were reported up to now [29–31]. Recently an X-ray crystallographic study of FabK from *S. pneumoniae* (SpFabK) (PDB id code: 2Z6I, 2Z6J) was reported [32], this was the unique FabK crystal structure published up to now. It gave a clear description of the active site of the target enzyme. Based on above information, we arranged a rational design approach to develop novel FabK inhibitors.

In the present study, we carried out molecular docking and pair interaction energy analysis to investigate the interaction mechanism between the active site of SpFabK and its ligands. Subsequently, the first FabK inhibitor 3D-QSAR model with comparative molecular field analysis (CoMFA) based on the molecular docking-based alignment was obtained, and then we sorted out six novel and potential inhibitor hits of SpFabK from the SPECs database [33] combining using the 3D-QSAR CoMFA predicted model, molecular docking, and FMO pair interaction energy analysis.

Materials and methods

Molecular docking

In order to explore the interaction mechanism and reasonable binding mode of ligands in the active site of SpFabK, molecular docking analysis was carried out by the FlexX module [34, 35] of SYBYL package [36]. The FlexX is a fast and automated docking program, which takes ligand's conformational flexibility into account during the docking process by an incremental fragment placing technique. We defined the active site as follows: all atoms located within the range of 6.5 Å from any atom of the TUI ligand (2-(4-(2-((3-(5-(pyridin-2-ylthio) thiazol-2-yl)ureido)methyl)-1H-imidazol-4-yl)phenoxy)acetic acid) were selected into the so-called active site, and the amino acid residue was, therefore, involved into the active site if at least one of its atoms was selected. The docking ligand was set as mol2 file type and assigned Gasteiger-Hückel charge, the input options for 3D coordinate generation of ligand was set as “If Necessary”,

formal charge assignment was set as “If Necessary”, add hydrogens was set as “Use Existing”, test atom typing was set as “No Testing (Assign Atom if Necessary)”, assign delocalized types was set as “Use Existing”. The output options for maximum number of poses per ligand was set as “30”, output format was set as “SYBYL Database”. Performing CScore calculations, the CScore execution mode was set as “Parallel” model.

FMO pair interaction analysis

To qualify and validate the interaction mechanism between the active site and ligands, *ab initio* fragment molecular orbital (FMO) calculations [37] were performed based on the ligand binding mode in the active site. FMO is an approximate molecular orbital method developed for the calculations of large molecules consisting of thousands of atoms. It has been successfully applied for the quantum mechanical calculations of binding energies and pair interaction energies of receptors-ligands [38, 39]. In the FMO method, the whole molecular system is divided into small fragments and *ab initio* FMO calculations are performed on fragments and fragment pairs, which are referred to as “monomers” and “dimers” respectively [40–42]. The total electronic energy of the molecular system is calculated by the following equation, where E_I , E_J and E_{IJ} are self-consistent field (SCF) energies of monomer (I), (J) and dimer (IJ), respectively.

$$E = \sum_I E_I + \sum_{I>J} (E_{IJ} - E_I - E_J) \quad (1)$$

Equation 1 can be transformed as follows

$$E = \sum_I E_I + \sum_{I>J} \Delta E_{IJ} \quad (2)$$

where ΔE_{IJ} is the pair interaction energy

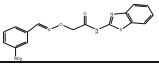
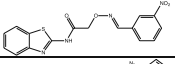
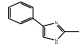
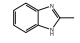
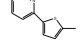
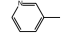
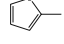
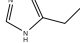
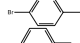
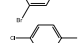
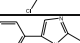
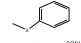
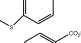
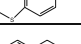
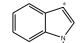
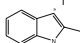
$$\Delta E_{IJ} = E_{IJ} - E_I - E_J \quad (3)$$

We adopted the residues located within a radius of 6.5 Å from the center of the complex of the docking ligand. The ends of the polypeptide fragments, –NH and –CO, were capped with hydrogen atoms. All FMO calculations in the present study were performed by using GAMESS software [43] at the restricted Hartree-Fock level with the 6–31G* basis set. Other adopted parameters are explained in detail shown as document elsewhere [44].

Data sets and molecular alignment rules for CoMFA modeling

The validation of 3D-QSAR CoMFA model is strongly dependent upon the selected training data set and molecular

Table 1 Molecular structural formulae of compounds collected for the 3D-QSAR CoMFA modeling

Compound	Structure	FabK pIC50	
B6		2.96	
AE848		2.29	
Compound	R1	FabK pIC50	
B24		4.06	
B36		3.13	
B37		2.47	
B38		1.64	
B39		1.52	
B40		1.49	
Compound	R2	FabK pIC50	
B29	H	2.16	
B32	6-OMe	2.70	
B33	6-Me	2.59	
B34	6-F	2.19	
B35	6-CN	2.35	
AG205	6-COOCH3	2.82	
Compound	R3	FabK pIC50	
B44	Ph	4.38	
B47		5.62	
B48		5.28	
B49		5.43	
Compound	R4	R5	FabK pIC50
B41	H	Ph	3.42
B43	H		4.43
B45	H		4.43
B46	H		4.01
Compound	R6	FabK pIC50	
A29		2.30	
A30		2.52	

alignment rule. All training data set twenty-two compounds (see Table 1 for specific molecular formula) with pIC50 values in a range from 1.49 to 5.62 were selected from the two references [29, 31]. Their biological inhibitory activi-

ties were determined by the same method. The testing set was constituted by AG205 and AE848 compound, they came from the references [45]. The three-dimensional structures of all compounds were obtained by using the

SYBYL program package. Partial atomic charges were calculated by the Gasteiger-Hückel method [46], and energy minimizations were performed using the Tripos force field [47] and the Powell conjugate gradient algorithm [48] with a convergence criterion of $0.05 \text{ kcal mol}^{-1} \text{ \AA}^{-1}$. All calculations were performed on a CCNUGrid-based computational environment (CCNUGrid web site: <http://202.114.32.71:8090/ccnu/chem/platform.xml>).

According to the previous study [44, 49], we learned that the molecular alignment obtained from molecular docking active conformation is more accurate and reliable. So in this study the molecular docking alignment rules were adopted. The active conformations of all compounds were achieved by FlexX, docking the ligand into the active site of SpFabK crystal structure, and the ligands' active conformations were selected from the binding orientation in the active site jointly evaluated by the consideration of FlexX energy scores.

CoMFA 3D-QSAR modeling

CoMFA steric and electrostatic interaction fields were calculated at each lattice intersection on a regularly spaced grid of 2 \AA . The grid pattern was generated automatically by the SYBYL/CoMFA routine. An sp^3 carbon atom with a *van der Waals* radius of 1.52 \AA and a $+1.0$ charge was used as the probe to calculate the steric (Lennard-Jones 6–12 potential) field and the electrostatic (Coulombic potential) field with a fixed dielectric constant at each lattice point. The electrostatic energy at the point where the steric energy exceeded the steric cutoff for any molecule in the analysis was set to the mean value of the non-excluded electrostatic field. Values of the steric and electrostatic fields were truncated at $30.0 \text{ kcal mol}^{-1}$.

A partial least-squares (PLS) approach [50, 51], which is an extension of the multiple regression analysis was used to derive the 3D-QSAR model, in which the CoMFA

descriptors were used as independent variables, and the experimental pIC_{50} values were used as dependent variables. The cross-validation with Leave-One-Out (LOO) option and the SAMPLS program [52] were applied to obtain the optimal number of components to be used in the final analysis. After the optimal number of components was determined a non-cross-validated analysis was performed without column filtering. The q^2 (cross-validated r^2), spress (cross-validated standard error of prediction), r^2 (non-cross-validated r^2), F values and standard error of estimate values were computed according to the definitions in SYBYL 7.0 package.

Molecular surface physicochemical properties

Surface physicochemical property maps, i.e., electrostatic potential, hydrophobic potential, and hydrogen bonding (donor/acceptor) potential maps of the SpFabK active site were generated on the solvent accessible (connolly) surface using the MOLCAD module [53] of SYBYL. These MOLCAD-generated property surface maps were compared and contrasted to those obtained by CoMFA modeling.

Virtual screening

To find some novel lead compounds with high potent inhibitory activity of SpFabK, structure-based virtual screening SPECS database [33] was carried out using FlexX docking. The SPECS database contained more than 1.5 million compounds offered by academia and research institutes from all over the world providing for drug discovery. The structure of the compounds from SPECS database are new, the compounds exhibit structural characteristics of a biologically active compound, and meet absorption distribution metabolism excretion (ADME) requirements. With the high-throughput virtual screening, the representative potential hit compounds were sorted out

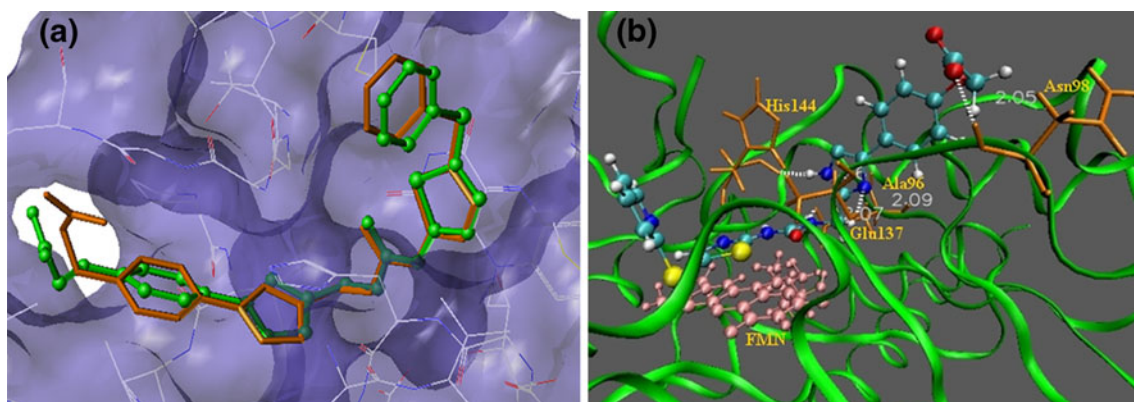
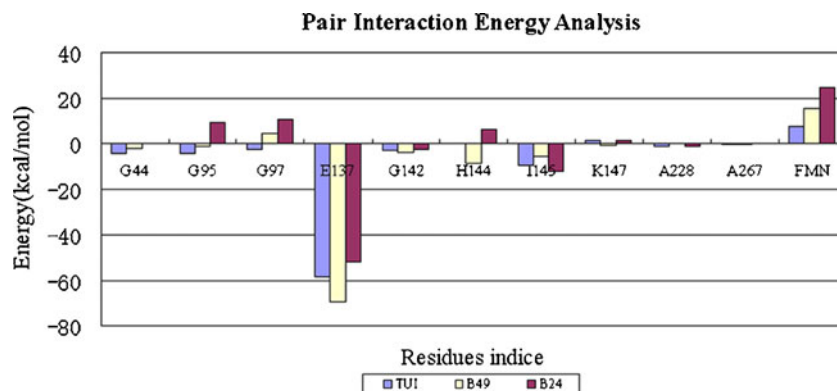


Fig. 1 (a) The superposition of docking mode of TUI (orange stick) and that binding mode in the crystal structure (green ball-and-stick). (b) The interaction analysis between the docking mode of TUI and the

active site of SpFabK (FMN: pink ball-and-stick; residues: orange stick; TUI: blue-green ball-and-stick)

Fig. 2 Pair interaction energies analyzed for compounds docking into the active site which were calculated at the FMO-RHF/6–31G* level (red: B24 compound; yellow: B49 compound; blue: TUI)



by jointly using the docking score, pair interaction analysis by FMO, predicted pIC50 values by CoMFA 3D-QSAR modeling, structural diversity, chemical and physical character.

Results and discussion

FMO pair interaction energy analysis based on molecular docking

In order to confirm the reliability of the docking procedure adopted herein, the initial geometric parameters of TUI (2-(4-(2-((3-(5-(pyridin-2-ylthio) thiazol-2-yl)ureido)methyl)-1H-imidazol-4-yl)phenoxy)acetic acid) backbone was extracted out of SpFabK crystal structure 2Z6J, added hydrogen atoms and subsequently submitted to a minimization by using the Tripos force field, and then it was docked back into the active site of 2Z6J (SpFabK) with the FlexX method. The structural parameters of enzyme were set rigidly while those ligands were set soft during the present molecular docking process. FlexX docking results showed that the binding position of TUI (shown in orange stick model) in the active site of SpFabK was indeed similar to that in the crystallographic complex structure

(shown in green ball-and-stick model, see Fig. 1a). The interaction analysis between the TUI ligand and the active site of SpFabK was illustrated in Fig. 1b, the TUI was shown in ball-and-stick, the thiazole ring and part of the ureido moiety of the TUI were involved in a face-to-face π - π stacking interaction with the isoalloxazine ring of FMN (flavin mononucleotide) shown in pink ball-and-stick. In addition, the thiazole group formed two hydrogen bindings interaction with Ala96 and His144 residues with the bonds distance being 1.96 Å and 2.09 Å, respectively; the ureido group and the carboxyl anion group formed hydrogen bindings to Glu137 and Asn98 residues with the bonds distance 2.07 Å and 2.05 Å, respectively. These information suggested that face-to-face π - π stacking and hydrogen-bonding play important roles during the complex forming. All the interaction analysis agreed with the structural features of the complex in reference [32], and the consistent results lent credibility to the docking process.

In order to validate numerically the results obtained from molecular docking with FlexX, and to detect important interactions between ligand and specific amino acid residues, FMO calculations were performed for a comparative study of pair interaction energies of ligand with the binding sites of SpFabK. The calculated pair interaction energies of TUI with individual residue fragments in the

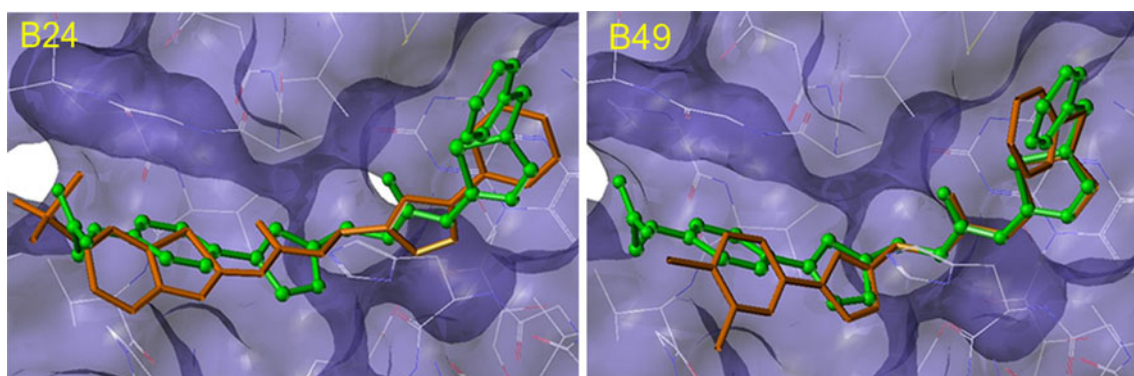


Fig. 3 The superposition of docking mode of B24 and B49 compound (orange stick) with TUI binding mode (green ball-and-stick) in the crystal structure, respectively

Table 2 Results summary of the CoMFA modeling with molecular dock-based alignments

	q^2	n	r^2	F	SE	E%	S%
Model-dock	0.511	4	0.986	307.181	0.166	59.0	41.0

N = the optimal number of components to be used in the final analysis. F = the ratio of r^2 to $1.0 - r^2$ (explained to unexplained), weighted so that the fewer the explanatory properties and the more the values of the target property, the higher the F ratio; SE: standard error. E%: contribution of electrostatic field; S%: contribution of steric field

selected active site of SpFabK were illustrated in Fig. 2. Of all amino acid residues located in the active site of SpFabK, the Glu137 fragment was responsible for the largest contribution to the stabilization due to the formation of hydrogen bonding of electrostatic interaction type between the TUI and the residues. The second largest contributors were His144 and Ile145 residues, which should be contributed to the electrostatic and non-polar interactions. The largest destabilization arose from FMN cofactor, due to the electrostatic interactions between the electronegative ureido moiety of the TUI and the electronegative isoalloxazine ring of FMN, and the contribution from the face-to-face π - π stacking interactions was ignored during the FMO calculation. As a further validation, the known inhibitors B24 and B49 compounds, with the pIC₅₀ values 4.06 and 5.43, respectively, acted as positive control, were docked into the active site of SpFabK. The two known inhibitors' binding modes in the active site and the pair interaction energies analysis between the two inhibitors and the active sites of SpFabK were shown in Figs. 2 and 3. Generally, all of the binding sites and the trends of pair interaction energies were similar to the complex crystal structure of SpFabK. The similar results lent credit and evidence to the reliability and reasonableness of the selected parameters in FlexX docking and the *ab initio* fragment molecular orbital (FMO) calculations in the present work.

3D-QSAR CoMFA modeling

Table 2 summarized the PLS analytical results for 3D-QSAR CoMFA modeling. Model-Dock model has cross-validated coefficients (q^2) up to 0.511 and regression coefficients (r^2) up to 0.986 with optimal number of components 4. The large q^2 value implied that the obtained CoMFA model was powerful in predicting pIC₅₀ values. Table 3 presented the predicted activity values and their residues from the experimentally measured pIC₅₀ for the selected 22 inhibitors of training set and two compounds of testing set. The numerical results in Table 2 showed that our present CoMFA model has good predictive ability. The predicted pIC₅₀ values were generally in good agreement with the experimental data with small residue (the relativity between predicted and experiment pIC₅₀ values was shown in Fig. S1). Model-dock model has high cross-validated

coefficient and powerful predicted ability, which validated the reliability of active conformations obtained by FlexX.

The 22 inhibitors alignment obtained by the molecular docking was shown in Fig. S2 of the Supporting information. Qualitatively, the steric and electrostatic fields derived from the docking-based alignment were a joint product by taking characters of both the ligands and the active site into account. Figure 4 showed the 3D steric and electrostatic maps derived from the CoMFA model using docking-based alignment. Compound B47, one of the most potent SpFabK

Table 3 Experimental activities, predicted activities and residual values predicted by the molecular alignment using active conformation achieved by molecular docking

Compound	pIC ₅₀		
	Actual	Predicted	Residues
B24	4.06	3.816	0.24
B29	2.16	2.076	0.08
B32	2.7	2.765	-0.07
B33	2.59	2.46	0.12
B34	2.19	2.513	-0.32
B35	2.35	2.461	-0.11
B36	3.13	3.071	0.06
B37	2.47	2.554	-0.09
B38	1.64	1.627	0.01
B39	1.52	1.652	-0.13
B40	1.49	1.363	0.13
B41	3.42	3.686	-0.27
B43	4.43	4.648	-0.22
B44	4.38	4.257	0.12
B45	4.43	4.446	-0.01
B46	4.01	4.135	-0.13
B47	5.62	5.464	0.16
B48	5.28	5.194	0.08
B49	5.43	5.47	-0.04
B06	2.96	2.827	0.13
A29	2.30	2.196	0.11
A30	2.52	2.394	0.13
AE848 ^t	2.29	2.38	0.09
AG205 ^t	2.82	2.71	0.11

^t testing set

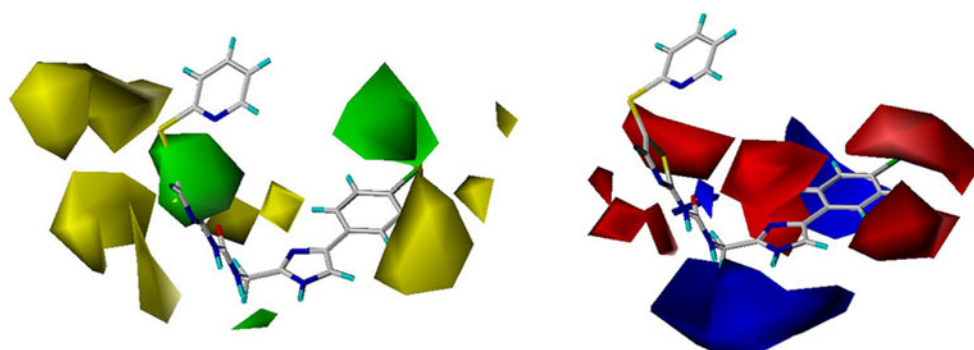


Fig. 4 Steric and electrostatic maps from the CoMFA model using docking-based active conformation alignment. Compound B47 was shown inside the field. Sterically favored areas (80% contribution) were represented by green polyhedra. Sterically disfavored areas (20%

contribution) were represented by yellow polyhedra. Blue contours (80% contribution) encompassed regions where an increase of positive charge will enhance affinity; whereas red contours (20% contribution) encompassed regions where an increase of negative charge will enhance affinity

inhibitor, was shown to be inside the fields. The contribution of the steric field to the activity was 41.0% and that of the electrostatic field was 59.0%. The 3D contour maps showed that the changes of molecular fields were associated with the differences of biological activity. The steric fields were in green and yellow. The regions of green contour suggested that more bulky substituents in these positions would improve the biological activity, while the yellow regions indicated that an increased steric bulk was unfavorable for the inhibitory activity.

The ureido moiety of compound B47 in Fig. 4 was located in the green region resulting in a higher pIC_{50} value of 5.62. The indole ring group of compound A29 was extended to the yellow region and therefore its pIC_{50} value was reduced to 2.30.

Figure 5a showed the steric contours projected over the solvent accessible (Connolly) topological surface (MOLCAD generated) of the active site of the SpFabK. The

yellow region (a) flanked the Pro118, Val116, and Gly97 residues, while the yellow region (b) flanked the His144 residues and the yellow region (c), (d) flanked the Leu266, Ala96, Gly95 residues and FMN cofactor, respectively. The green region was located in the channels and toward outside of the active site pocket. These steric field distributions of CoMFA model (Model-dock) guaranteed a large percentage of the ligand volume buried inside the binding pocket [54].

Figure 5b showed the electrostatic contours projected over the electrostatic potential surface (MOLCAD generated) of the active site of the SpFabK. The CoMFA electrostatic fields in blue suggested that the positive charged substitutions may increase the inhibitory activity, while the red region indicated that a high electronic density may play a favorable role in inhibitory potency. The blue regions of the MOLCAD generated contour maps represent a negative electrostatic potential, the red regions represented a positive

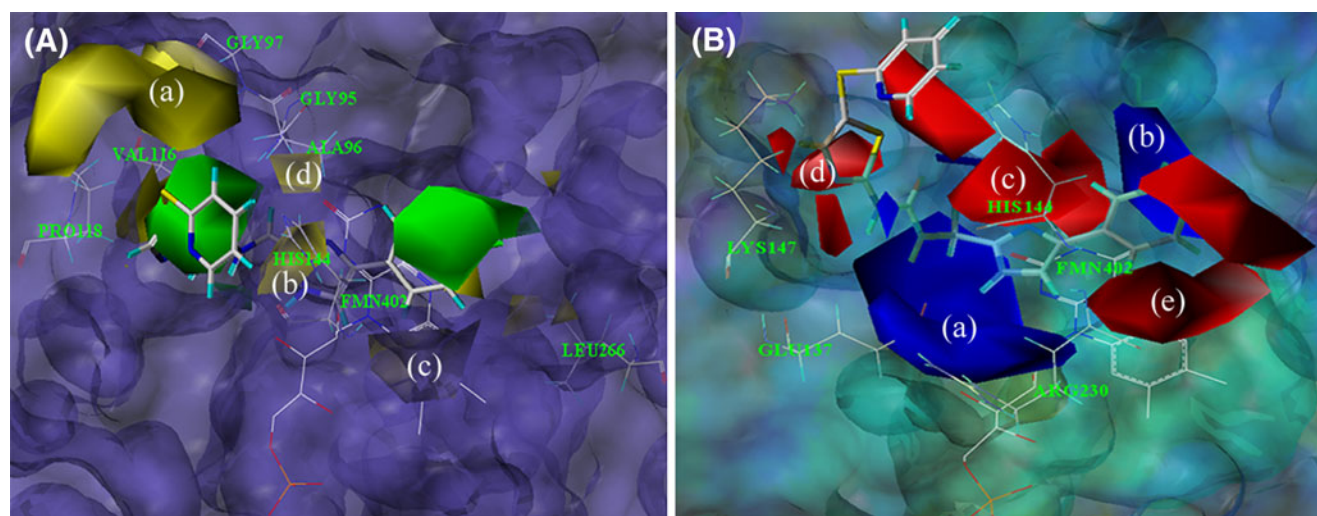


Fig. 5 (a) Steric contours projected over the solvent accessible (Connolly) topological surface (MOLCAD generated) of the active site of the SpFabK; (b) Electrostatic contours projected over the

electrostatic potential surface (blue, negative potential; red/brown, positive potential) of the active site of the SpFabK

Table 4 Total scores of FlexX and the predicted pIC50 of CoMFA for six selected hit compounds and known inhibitor TUI compound

Compound	135385	115534	30728	131229	44219	93008	TUI
Scores	10.18	9.52	8.88	8.59	8.42	7.92	8.47
Predicted pIC50 value	4.54	3.45	4.24	4.39	3.75	4.86	4.50

electrostatic potential. The large blue regions (a) and (b) of CoMFA contour match well with the blue (highly electro-negative) surface of the binding sites provided by the Glu137 residues, and the FMN cofactor. Also, the red regions (c), (d), and (e) of CoMFA contour matched well with the red (electropositive) surface of the binding sites provided by the guanidine groups of the His144, Lys147 and Arg230 residues. The comparison of the two types of contour maps showed that the present docking-based CoMFA model generally agree well with the active sites of the SpFabK in the present work.

Virtual screening

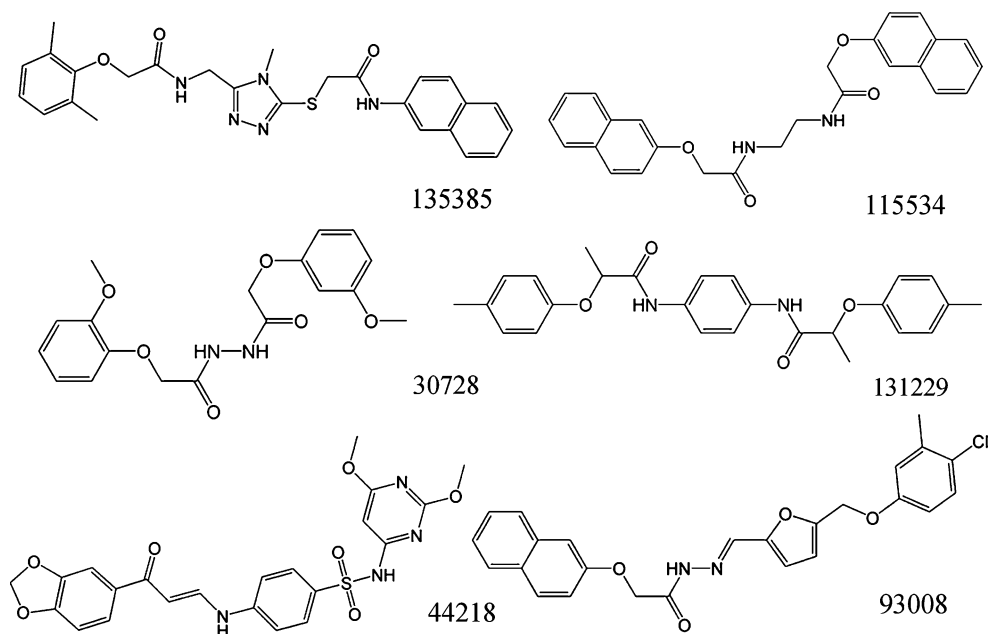
Discovering novel lead compounds is the key and starting point for any new drug research and development project. SpFabK structure-based high throughput virtual screening was carried out by FlexX method in the present study. All the docking selected parameters in FlexX were set as above. Before the docking process, all compounds from SPECS database were transformed from 2D to 3D by CONCORD module [55] of SYBYL7.0. Partial charges were assigned to the atoms according to the method of Gasteiger-Hückel [46] implemented in SYBYL 7.0. To control the performance of the docking strategy, three known SpFabK inhibitors with high pIC50 values,

B47, B48 and B49 were added into the search samples, their appearance in the hit list served to calibrate and validate the high throughput virtual screening approach. After above processes, all compounds were prepared for the following FlexX docking study, the docking process as performed above. According to the lowest docking score of the three known inhibitors, the 4909 entries with docking score more than 6.90 were primitively screened out for further analysis.

The above obtained docking-based CoMFA 3D-QSAR model associated the character of ligand and target, so it has effective predicted capability. However, FlexX score is sensitive to the hydrogen bond formation, putting higher weights on this term than to the steric effect on the activity. Thus the predicted pIC50 value by CoMFA would complement and validate the score results of FlexX. At this step, the pIC50 values of all the 4909 entries with the binding mode in the active site of SpFabK were predicted with the CoMFA 3D-QSAR model. We put more confidence on those entries with higher scores from both CoMFA modeling and FlexX docking.

According to the predicted pIC50 values and docking scores, 87 entries with higher scores of CoMFA modeling and FlexX docking were selected. And then the binding mode analysis, structure diversity, chemical and physical character analysis were performed on the 87 entries.

Fig. 6 Molecular structural formulae of hit compounds sorted out by virtual screening



Finally, the representative six potential hit compounds were sorted out by jointly using the FlexX docking score, predicted pIC50 values, *ab initio* FMO calculations, binding mode, structural diversity, chemical and physical characteristics. Table 4 depicted the structures of six potential hit compounds with higher predicted pIC50 values and docking score of FlexX. As shown in Fig. 6, the structures backbone of all these compounds were different from the known inhibitors, but they had similar binding modes and FMO pair interaction energy trends in the active site of SpFabK.

Conclusions

In the present study, the interaction mechanism and pair interaction energies of ligand with the active site of SpFabK were analyzed with the *ab initio* FMO calculation based on the FlexX docking model at the FMO-RHF/6–31G* level. Most of the binding sites and the trends of pair interaction energies were similar, which lent credit to the reliability of the *ab initio* FMO calculation and illustrated the reasonableness of the selected parameters in molecular docking in the present work. With the above docking process, a molecular docking-based 3D-QSAR CoMFA model of FabK inhibitors with excellent cross-validated q^2 and non-cross-validated r^2 values were established for the first time. Subsequently, integrating of the 3D-QSAR CoMFA predicted model, molecular docking and FMO pair interaction analysis structure-based inhibitor virtual screening have been performed. And finally six novel and potential inhibitor hits of SpFabK with high screening scores were sorted out for further study.

Acknowledgments This work was supported by the Natural Science Foundation of China (No. 30900935), the Chinese Post-doctoral Research Fund Special Funded Projects (No. 200902442), and the China Postdoctoral Science Foundation Funded Project (No. 20080440140). We thank Prof. Wan of Central China Normal University for providing the computer modeling supporting.

References

- John LA, Kristina D, Thomas SL (2004) Streptococcus pneumoniae isoprenoid biosynthesis is downregulated by Diphosphomevalonate: an antimicrobial target. *Biochemistry* 43:16461–16466
- Bartlett JG, Breiman RF, Mandell LA, File TM Jr (1998) Community-acquired pneumonia in adults: Guidelines for management The Infectious Diseases Society of America. *Clin Infect Dis* 26:811–838
- Cohen ML (1992) Epidemiology of drug resistance: Implications for a post-antimicrobial era. *Science* 257:1050–1055
- Johnson CN, Briles DE, Benjamin WH Jr, Hollingshead SK, Waites KB (2005) Relative fitness of fluoroquinolone-resistant Streptococcus pneumoniae. *Emerg Infect Dis* 11:814–820
- Shinefield HR, Black S (2000) Efficacy of pneumococcal conjugate vaccines in large scale field trials. *Pediatr Infect Dis J* 19:394–397
- Cronan JE (2006) Remarkable structural variation within fatty acid megasynthases. *Nat Chem Biol* 2:232–234
- Maier T, Jenni S, Ban N (2006) Architecture of mammalian fatty acid synthase at 45 Å resolution. *Science* 311:1258–1262
- Massengo-Tiass RP, Cronan JE (2009) Diversity in enoyl-acyl carrier protein reductases. *Cell Mol Life Sci* 66:1507–1517
- Heath RJ, Rock CO (1995) Enoyl-acyl carrier protein reductase (fabI) plays a determinant role in completing cycles of fatty acid elongation in Escherichia coli. *J Biol Chem* 270:26538–26542
- Heath RJ, Rock CO (1996) Regulation of fatty acid elongation and initiation by acyl-acyl carrier protein in Escherichia coli. *J Biol Chem* 271:1833–1836
- George N, Colin AS, Edinson L, Mack RK, David AF, James CS, Ruben A (2007) Discovery of novel inhibitors targeting enoyl-acyl carrier protein reductase in plasmodium falciparum by structure-based virtual screening. *Biochem Biophys Res Commun* 358:686–691
- Heath RJ, Rock CO (2000) A triclosan-resistant bacterial enzyme. *Nature* 406:145–146
- Heerding DA, Chan G, DeWolf WE, Fosberry AP, Janson CA, Jaworski DD, McManus E, Miller WH, Moore TD, Payne DJ (2001) 1, 4-Disubstituted imidazoles are potential antibacterial agents functioning as inhibitors of enoyl-acyl carrier protein reductase (FabI). *Bioorg Med Chem Lett* 11:2061–2065
- Seefeld MA, Miller WH, Newlander KA, Burgess WJ, Payne DJ, Rittenhouse SF, Moore TD, DeWolf WE Jr, Keller PM, Qiu X, Janson CA, Vaiday K, Fosberry AP, Smyth MG, Jaworski DD, Slater-Radosti C, Huffman WF (2001) Inhibitors of bacterial enoyl-acyl carrier protein reductase (FabI): 29-Disubstituted 1234-tetrahydropyrido[3,4-b]indoles as potential antibacterial agents. *Bioorg Med Chem Lett* 11:2241–2244
- Ling LL, Xian J, Ali S, Geng B, Fan J, Mills DM, Arvanites AC, Orgueira H, Ashwell MA, Carmel G, Xiang YT, Moir D (2004) Identification and characterization of inhibitors of bacterial enoyl-acyl carrier protein reductase. *Antimicrob Agents Chemother* 48:1541–1547
- Kitagawa H, Ozawa T, Takahata S, Iida M, Saito J, Yamada M (2007) Phenylimidazole derivatives of 4-pyridone as dual inhibitors of bacterial enoyl-acyl carrier protein reductases FabI and FabK. *J Med Chem* 50:4710–4720
- Takahata S, Iida M, Yoshida T, Kumura K, Kitagawa H, Hoshiko S (2007) Discovery of 4-pyridone derivatives as specific inhibitors of enoyl-acyl carrier protein reductase (FabI) with antibacterial activity against Staphylococcus aureus. *J Antibiot* 60:123–128
- Yum JH, Kim CK, Yong D, Lee K, Chong Y, Kim CM, Kim JM, Ro S, Cho JM (2007) In vitro activities of CG400549 a novel FabI inhibitor against recent clinical staphylococcal isolates in Korea. *Antimicrob Agents Chemother* 51:2591–2593
- Gita SR, Rajakrishnan V, Manoj K (2008) Structure-based design of a novel class of potent inhibitors of InhA the Enoyl Acyl Carrier Protein Reductase from Mycobacterium Tuberculosis: A Computer Modelling Approach. *Chem Biol Drug Des* 72:444–449
- Kumar A, Siddiqi MI (2008) CoMFA based de novo design of Pyrrolidine Carboxamides as Inhibitors of Enoyl Acyl Carrier Protein Reductase from Mycobacterium tuberculosis. *J Mol Model* 14:923–935
- Rozwarski DA, Grant GA, Barton DH, Jacobs WR, Sacchettini JC (1998) Modification of the NADH of the isoniazid target (InhA) from Mycobacterium tuberculosis. *Science* 279:98–102v
- Baldock C, Rafferty JB, Sedelnikova SE, Baker PJ, Stuitje AR, Slabas AR, Hawkes TR, Rice DW (1996) A mechanism of drug action revealed by structural studies of enoyl reductase. *Science* 274:2107–2110

23. Levy CW, Baldock C, Wallace AJ, Sedelnikova S, Viner RC, Clough JM, Stuitje AR, Slabas AR, Rice DW, Rafferty JB (2001) A study of the structure-activity relationship for diazaborine inhibition of *Escherichia coli* enoyl-ACP reductase. *J Mol Biol* 309:171–180
24. McMurry LM, Oethinger M, Levy SB (1998) Triclosan targets lipid synthesis. *Nature* 394:531–532
25. Heath RJ, Yu YT, Shapiro MA, Olson E, Rock CO (1998) Broad spectrum antimicrobial biocides target the FabI component of fatty acid synthesis. *J Biol Chem* 273:30316–30320
26. Levy CW, Roujeinikova A, Sedelnikova S, Baker PJ, Stuitje AR, Slabas AR, Rice DW, Rafferty JB (1999) Molecular basis of triclosan activity. *Nature* 398:383–384
27. Ward WH, Holdgate GA, Rowsell S, McLean EG, Pauptit RA, Clayton E, Nichols WW, Colls JG, Minshull CA, Jude DA, Mistry A, Timms D, Camble R, Hales NJ, Britton CJ, Taylor IW (1999) Kinetic and structural characteristics of the inhibition of enoyl (acyl carrier protein) reductase by triclosan. *Biochemistry* 38:12514–12525
28. Stewart MJ, Parikh S, Xiao G, Tonge PJ, Kisker C (1999) Structural basis and mechanism of enoyl reductase inhibition by triclosan. *J Mol Biol* 290:859–865
29. Seefeld MA, Miller WH, Newlander KA, Burgess WJ, DeWolf WE Jr, Elkins PA, Head MS, Jakas DR, Janson CA, Keller PM, Manley PJ, Moore TD, Payne DJ, Pearson S, Polizzi BJ, Qiu XY, Rittenhouse SF, Uzinskas IN, Wallis NG, Huffman WF (2003) Indole naphthyridinones as inhibitors of bacterial enoyl-ACP reductases FabI and FabK. *J Med Chem* 46:1627–1635
30. Zheng CJ, Sohn MJ, Kim WG (2006) Atromentin and leucomelone the first inhibitors specific to enoyl-ACP reductase (FabK) of *Streptococcus pneumoniae*. *J Antibiot* 59:808–812
31. Ozawa T, Kitagawa H, Yamamoto Y, Takahata S, Iida M, Osakib Y, Yamada K (2007) Phenylimidazole derivatives as specific inhibitors of bacterial enoyl-acyl carrier protein reductase FabK. *Bioorg Med Chem* 15:7325–7336
32. Saito J, Yamada M, Watanabe T, Iida M, Kitagawa H, Takahata S, Ozawa T, Takeuchi Y, Ohsawa F (2008) Crystal structure of enoyl-acyl carrier protein reductase (FabK) from *Streptococcus pneumoniae* reveals the binding mode of an inhibitor. *Protein Sci* 17:691–699
33. Specs (1987) <http://www.specs.net>
34. Rarey M, Kramer B, Lengauer T, Klebe G (1996) A Fast Flexible Docking Method Using an Incremental Construction Algorithm. *J Mol Biol* 261:470–489
35. Kramer B, Rarey M, Lengauer T (1999) Evaluation of the FlexX Incremental Construction Algorithm for Protein-Ligand Docking. *Proteins* 37:228–241
36. SYBYL7.0 (2003) Tripos Inc St Louis Missouri USA
37. Fukuzawa K, Kitaura K, Nakata K, Kaminuma T, Nakano T (2003) Workshop 15 Fragment molecular orbital study of the binding energy of ligands to the estrogen receptor. *Pure Appl Chem* 75:2405–2410
38. Nemoto T, Fedorov DG, Uebayasi M, Kanazawa K, Kitaura K, Komeiji Y (2005) Ab initio fragment molecular orbital (FMO) method applied to analysis of the ligand-protein interaction in a pheromone-binding protein. *Comput Biol Chem* 29:434–439
39. Yamagishi K, Yamamoto K, Yamada S, Tokiwa H (2006) Functions of key residues in the ligand-binding pocket of vitamin D receptor: Fragment molecular orbital-interfragment interaction energy analysis. *Chem Phys Lett* 420:465–468
40. Kitaura K, Ikeo E, Asada T, Nakano T, Uebayasi M (1999) Fragment molecular orbital method: an approximate computational method for large molecules. *Chem Phys Lett* 313:701–706
41. Komeiji Y, Inadomi Y, Nakano T (2004) PEACH 4 with ABINIT-MP: a general platform for classical and quantum simulations of biological molecules. *Comput Biol Chem* 28:155–161
42. Nakano T, Kaminuma T, Sato T, Fukuzawa K, Akiyama Y, Uebayasi M, Kitaura K (2002) Fragment molecular orbital method: use of approximate electrostatic potential. *Chem Phys Lett* 351:475–480
43. Schmidt MW, Baldrige KK, Boatz JA, Elbert ST, Gordon MS, Jensen JH, Koseki S, Matsunaga N, Nguyen KA, Su S, Windus TL, Dupuis M, Montgomery JA (1993) General atomic and molecular electronic-structure system. *J Comput Chem* 14:1347–1363
44. Zhang QY, Yang JY, Liang K, Feng LL, Li SP, Wan J, Xu X, Yang GF, Liu D, Yang S (2008) Binding interaction analysis of the active site and its inhibitors for neuraminidase (N1 subtype) of human influenza virus by the integration of molecular docking FMO calculation and 3D-QSAR CoMFA modeling. *J Chem Inf Model* 48:1802–1812
45. Takahata S, Iida M, Osaki Y, Saito J, Kitagawa H, Ozawa T, Yoshida T, Hoshiko S (2006) AG205, a novel agent directed against FabK of *Streptococcus pneumoniae*. *Antimicrob Agents Chemother* 50:2869–2871
46. Gasteiger J, Marsili M (1980) Iterative Partial Equalization of Orbital Electronegativity - A Rapid Access to Atomic Charges. *Tetrahedron* 36:3219–3228
47. Clark M, Cramer RD, van Opdenbosch N (1989) The Tripos Force Field. *J Comput Chem* 10:982–1012
48. Powell MJD (1977) Restart Procedures for the Conjugate Gradient Method. *Math Program* 12:241–254
49. Zhang QY, Wan J, Xu X, Yang GF, Ren YL, Liu JJ, Wang H, Guo Y (2007) Structure-based rational quest for potential novel inhibitors of human HMG-CoA reductase by combining CoMFA 3D QSAR modeling and virtual screening. *J Comb Chem* 9:131–138
50. Wold S, Rhue A, Wold H, Dunn WJI (1984) The covariance problem in linear regression The partial least squares (PLS) approach to generalized inverses. *SIAM J Sci Statist Comput* 5:735–743
51. Clark M, Cramer RD (1993) The probability of chance correlation using partial least squares (PLS). *Quant Struct Act Relat* 12:137–145
52. Bush BL, Nachbar RB (1993) Sample-distance partial least-squares PLS optimized for many variables with application to CoMFA. *J Comput Aided Mol Des* 7:587–619
53. Waldherr-Teschner M, Goetze T, Heiden W, Knoblauch M, Vollhardt H, Brickmann J (1992) MOLCAD - computer aided visualization and manipulation of models in molecular science. In: Post FH, Hin AJS (eds) *Advances in scientific visualization*. Springer, Heidelberg, Germany, pp 8–67
54. Sulpizi M, Folkers G, Rothlisberger U, Carloni P, Scapozza L (2002) Applications of density functional theory-based methods in medicinal chemistry. *Quant Struct Act Relat* 21:173–181
55. Rusinko IIIA, Skell JM, Balducci R (1988) CONCORD. University of Texas Austin TX and Tripos Associates St Louis MO